Journal of Power Sources 260 (2014) 82–88

Contents lists available at ScienceDirect

Journal of Power Sources

journal homepage: www.elsevier.com/locate/jpowsour

Electrocatalytic performance of carbon supported Pd catalyst modified with Keggin type of Sn-substituted polyoxometalatate for formic acid oxidization

Yun Ji, Liping Shen, Anxing Wang, Min Wu, Yawen Tang, Yu Chen, Tianhong Lu*

Jiangsu Key Laboratory of New Power Batteries, College of Chemistry and Materials Science, Nanjing Normal University, Nanjing 210023, PR China

HIGHLIGHTS

- The new polyoxometallate $K_7Co^{II}W_{11}O_{39}Sn^{IV}OH$ has Keggin type of Sn-substituted structure.
- The Pd/C–K_7 catalyst is prepared with the simple impregnation–reduction method.
- The Pd/C–K_7 catalyst inhibits the CO pathway for the oxidation of formic acid.
- The Pd/C–K_7 catalyst exhibits enhanced stability and activity for the formic acid oxidation.

ARTICLE INFO

Article history:
Received 13 November 2013
Received in revised form
11 February 2014
Accepted 7 March 2014
Available online 15 March 2014

Keywords:
Formic acid oxidation
Carbon supported Pd catalyst
Polyoxometalate
Electrocatalytic activity
Direct formic acid fuel cells

ABSTRACT

The carbon supported Pd(Pd/C) catalyst modified by the new polyoxometalate with Keggin type of Sn-Substituted structure $K_7Co^{II}W_{11}O_{39}Sn^{IV}OH$ (Pd/C–K_7) catalyst is prepared with the simple impregnation–reduction method. This work investigates the effects of Pd/C–K_7 catalyst for direct formic acid fuel cells (DFAFCs). The morphology, structure, size and composition of the Pd/C–K_7 catalyst are characterized by transmission electron microscopy (TEM) energy dispersive spectrum (EDS), X-ray diffraction (XRD). Cyclic voltammetry, chronoamperometry and CO-stripping voltammetry tests demonstrate the Pd/C–K_7 catalyst have higher electrocatalytic activity, better electrochemical stability, and higher resistance to CO poisoning over the unmodified Pd/C catalyst for the formic acid oxidation reaction (FAOR) owing to $K_7Co^{II}W_{11}O_{39}Sn^{IV}OH$ with Keggin structure. Therefore, the Pd/C–K_7 catalyst could be used as the excellent anodic catalyst in DFAFCs.

1. Introduction

With low fuel crossover and high energy density, DFAFCs are expected to be among the first commercial applications of various fuel cells [1–5]. Formic acid electrooxidation obeys a triple-path mechanism in acidic electrolyte (Scheme 1) [6–9], namely: (i) a direct pathway, in which formic acid is oxidized directly into CO_2; (ii) an indirect pathway, via CO_{ads} formation and oxidation; (iii) a formate pathway, involving the formation and subsequent oxidation of formate to CO_2. The efficiency of the formic acid electrooxidation reaction is highly dependent on the catalyst and Pd-catalyzed formic acid electrooxidation reaction is one of the most important reactions in DFAFCs. Unfortunately, the electrocatalytic stability of the Pd catalyst for formic acid is poor owing to the poisoning adsorption of CO_{ads} via the indirect pathway [10]. Therefore, improving the resistance of the Pd catalyst to the poisoning species is a preferable method for alleviating the deactivation of the Pd catalyst compared with the oxidative treatment [11,12].

Further studies have revealed that Pd catalyst is bifunctional [13]. On the other hand, it can simultaneously catalyze the electrooxidation and decomposition of formic acid. The decomposition of formic acid over the Pd catalyst could undergo through two parallel pathways [14,15]:

$$HCOOH \rightarrow CO_2 + H_2 \quad \text{(dehydrogenation)} \tag{1}$$

$$HCOOH \rightarrow CO + H_2O \quad \text{(dehydration)} \tag{2}$$

The decomposition of formic acid over the Pd catalyst could waste a lot of formic acid and produce CO in dehydration reaction

* Corresponding author. Tel.: +86 13809029980; fax: +86 25 85891767.
E-mail address: tianhonglu107111@163.net (T. Lu).

http://dx.doi.org/10.1016/j.jpowsour.2014.03.024
0378-7753/

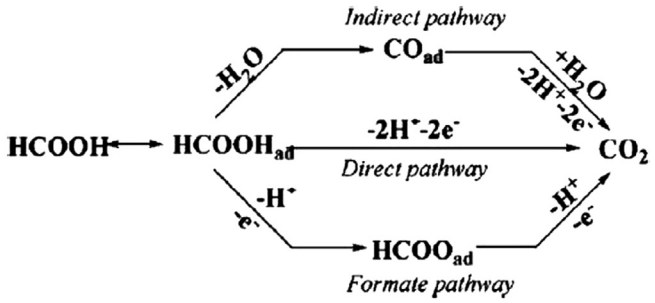

Scheme 1. Schematic description of the "triple-path way" reaction mechanism for the formic acid oxidation.

(2). Furthermore, the produced CO would poison the Pd catalyst and decreases its electrocatalytic performance. Therefore, reducing the decomposition of formic acid over the Pd catalyst is also a good method to improve the electrocatalytic performance of the Pd catalyst.

The polyoxometallate often serves as the acid catalyst due to its acidity. It can be also used to catalyze alcohol compounds for its good performance of oxidation–reduction [16,17]. On the other hand, metal-substituted derivative of the polyoxometallate has so many characteristics, such as highly stable redox state, adjustable redox voltage and multielectron transfer, which has been widely used in the field of catalysis and electrochemistry [18]. The new polyoxometallate with Keggin structure is widely investigated and the anion's general structural formula is $[XM_{12}O_{40}]^{n-}$ (X = P, Si, Co, Ge, Ga, As, Zn, M = metal or organo-metallic) [19–21]. According to the previous reports that tin suppresses CO buildup on platinum surfaces [22,23], and then tin has been shown to promote formic acid oxidation on palladium to also to irreversibly adsorb on a palladium surface [11,24,25].

In this paper, the inorganic substances $SnCl_4$ is used to synthesize the new polyoxometallate, which hasn't been reported. Then, Pd/C–K_7 catalyst was prepared with the simple impregnation–reduction method and the electrocatalytic performance of the Pd/C–K_7 catalyst for formic acid oxidation was investigated. The results indicated that the Pd/C–K_7 catalyst shows the excellent electrocatalytic performance for formic acid oxidation. This is meaningful for DFAFC because such catalyst would simultaneously solve two big problems: the poor electrocatalytic performance of the Pd catalyst and the decomposition of formic acid over the Pd catalyst.

2. Experimental

2.1. Reagents and chemicals

Vulcan XC-72 carbon was obtained from Cabot Company (Boston, USA). $PdCl_2$ was purchased from Sinopharm Chemical Reagent Co. Ltd. (Shanghai, China). 5 wt% Nafion solution was purchased from Aldrich Chemical CO, USA. All other reagents were of analytical grade and used without further purification. All the aqueous solutions were prepared with Millipore water (Purelab Classic Corp., USA).

2.2. Preparation of catalysts

The $K_7Co^{II}W_{11}O_{39}Sn^{IV}OH$ was prepared as follows: 36.4 g $Na_2WO_4 \cdot 2H_2O$ was dissolved in 200 mL H_2O and pH of the solution was adjusted to 6 with the glacial acetic acid. The solution was heated until boiling. Then, 40 mL aqueous solution with 2.4 g $Co(Ac)_2 \cdot 4H_2O$ and the 10 mL aqueous solution with 7.2 g $SnCl_4 \cdot 5H_2O$ was respectively injected dropwise into the boiling solution. After the pH of the mixed solution was adjusted to 2 with 4 M HCl, the temperature of the solution was kept at 80–90 °C for 1 h. Then, the mixed solution was added into 11.9 g KCl and stirred for 1 h. Finally, the blue precipitate was obtained, which was filtered, washed and dried at room temperature for 12 h.

The Pd/C catalyst with 20.0 wt% Pd was prepared with the following procedure: 3.13 mL 0.04504 M $PdCl_2$ and 60 mg Vulcan XC-72 carbon were mixed with water to the final volume of 10 mL. The resulting suspension was sonicated for 30 min and stirred mechanically for 4 h. After the pH of the suspension was adjusted to 8–9 with the Na_2CO_3 solution, the appropriate amount of $NaBH_4$ solution was slowly added to the suspension and then, the suspension was stirred for 1 h. Finally, after the mixture was washed, filtered and dried in a vacuum oven at 50 °C for 12 h, the Pd/C catalyst was obtained.

The Pd/C–K_7 catalyst was prepared as follows: 50 mg Pd/C catalyst was immersed in 1.5×10^{-4} M $K_7Co^{II}W_{11}O_{39}Sn^{IV}OH$ solution. The suspension was continuously stirred for 6 h. Finally, after the mixture was washed, filtered and dried in a vacuum oven at 50 °C for 12 h, the Pd/C–K_7 catalyst was obtained.

2.3. Characterizations of catalysts

The chemical structure and elemental analysis of the synthesized $K_7Co^{II}W_{11}O_{39}Sn^{IV}OH$ polyoxometallate were characterized by a Tensor-27 FT-IR (Bruker, Germany) with the scanned area from 400 to 4000 cm^{-1} and resolution ratio was 4 cm^{-1} and a Intrepid-II ICP-AES (Thermo Elemental, USA). The catalyst composition was determined using the energy dispersive spectrometer (EDS) with Vantage Digital Acquisition Engine (Thermo Noran, USA). X-ray diffraction (XRD) patterns were obtained on a Model D/max-rC X-ray diffractometer with the Cu K_α (λ = 1.5406 Å) radiation source operating at 40 kV and 100 mA. The morphology and particle size of the Pd/C and Pd/C–K_7 catalysts were investigated using a JEOL JEM-2010 transmission electron microscopy (TEM) operated at 200 kV.

2.4. Electrochemical measurements

The electrochemical measurements were carried out at 30 ± 1 °C with CHI600B electrochemical analyzer in the electrochemical cell with the conventional three electrodes. The Pt plate was used as the auxiliary electrode. The saturated calomel electrode (SCE) was used as the reference electrode. All the potentials were quoted with respect to SCE. The working electrodes were prepared as follows: A glassy carbon electrode was polished sequentially with 0.3 and 0.05 μm Al_2O_3, followed by a wash. 8 mg catalyst and 4 mL C_2H_5OH were mixed to obtain the catalyst slurry. Then, 8.9 μL slurry was spread on the surface of the glassy carbon electrode. After drying, 4.5 μL Nafion solution was used to cover the surface of the catalyst layer. The diameter of the glassy carbon electrode is 4 mm with the geometric surface area of 0.1256 cm^2. The specific loading of the catalyst on the electrode surface was 28 μg cm^{-2}. The Pd/C and Pd/C–K_7 catalyst electrodes were cleaned electrochemically before use. In order to clean the electrode, the cyclic voltammetric treatment of the Pd/C or Pd/C–K_7 catalyst electrode was taken from −0.2 V to 0.8 V in 0.5 M H_2SO_4 solution.

For electrochemical measurements, the electrolyte is 0.5 M H_2SO_4 solution with or without 0.5 M HCOOH. The chronoamperometric experiments were performed in 0.5 M H_2SO_4 and 0.5 M HCOOH solution at a potential of 0.1 V for 3000 s. Prior to the measurements, a steady stream of N_2 was bubbled into the solution for 10 min to remove O_2 dissolved in the electrolyte. During the measurement, N_2 was flowed above the solution. For the electrochemical measurement of the adsorbed CO, the electrode potential

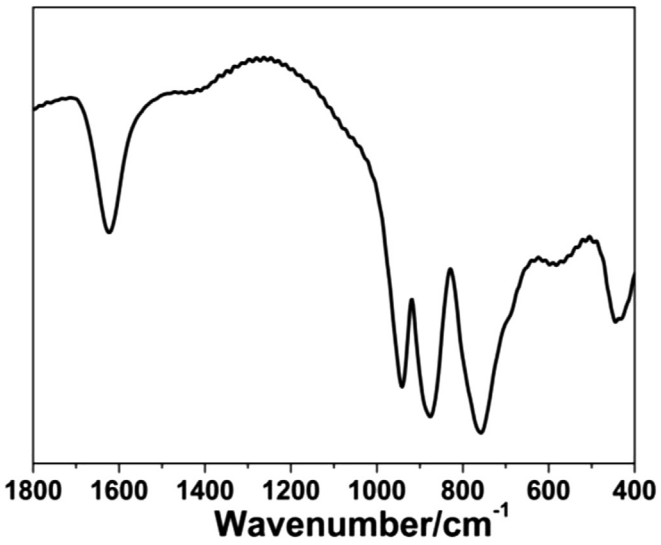

Fig. 1. FT-IR spectrum of $K_7Co^{II}W_{11}O_{39}Sn^{IV}OH$.

was fixed at 0 V and CO was bubbled into the electrolyte for 15 min until CO was fully adsorbed on the electrode [26,27]. Then, N_2 was bubbled into the solution for 10 min to remove CO in the solution.

2.5. Measurement of decomposition of formic acid

20 mg Pd/C or Pd/C–K_7 catalyst, 30 mL 0.5 M HCOOH and 0.5 M H_2SO_4 solution were added into a three-necked flask. The gases produced can be collected between 28 °C and 29 °C from the water bath under continuous stirring condition. Then, the volume of gas produced from decomposition of formic acid over the catalyst was recorded every 5 min for 2 h.

3. Results and discussion

3.1. Catalysts characterization

The FT-IR spectra of new polyoxometalate with Keggin structure (Fig. 1) shows that fingerprints (1200–400 cm^{-1}) of the polyoxmetalate existed four characteristic peaks, ν_{as}(W–O_d), ν_{as}(W–O_b–W), ν_{as}(W–O_c–W) and δ(Co–O_a). Three bands at 943, 873 and 760 cm^{-1} can be assigned to antisymmetric and stretching vibrations of W=O_d, W–O_b–W and W–O_c–W, respectively [28–30]. The band at 442 cm^{-1} arised from the flexural vibration of O–C_O–O [31]. These infrared results demonstrate that the new polyoxometalate possesses Keggin structure. The composition of the new polyoxometalate is analyzed by ICP measurement. The results shows the actual mass fractions of the metal elements K, Co, W, Sn are 8.17%, 1.21%, 64.06% and 3.97% respectively, which are close to the theoretical values: 8.76%, 1.89%, 64.96% and 3.82%. Therefore the corresponding formula is $K_7Co^{II}W_{11}O_{39}Sn^{IV}OH$.

The primary Keggin structure was shown as Fig. 2A and the structure was changed after the introduction of tin element [32,33]. As shown in the structure of the new polyoxometalate (Fig. 2B), the Co lied in the center of the tetrahedron, While the Sn entered into the position of octahedron. The new polyoxometalate consists multiple transition metal ion of high protonic conductivity. Then the high ionic conductivity of the new polyoxometalate can enhance the conductivity of the electrode and promote electron transfer reactions [12,34,35].

The composition and structure of the Pd/C–K_7 catalyst were investigated by EDS and XRD. As shown by the EDS spectra of the Pd/C–K_7 catalyst (Fig. 3A). The co-existence of Co, W, Sn, Pd and C characteristic peaks were observed in the Pd/C–K_7 catalyst. Since only $K_7Co^{II}W_{11}O_{39}Sn^{IV}OH$ molecule contains Co, W and Sn elements, this result indicated that the Pd/C catalyst is indeed modified by $K_7Co^{II}W_{11}O_{39}Sn^{IV}OH$. In the XRD pattern (Fig. 3B) of the Pd/C–K_7 catalyst, the characteristic peak at 25°belong to the C (002) plane and other diffraction peaks at 39.8°, 44.9°, 67.6°, and 81.2° can be indexed to Pd (111), (200), (220) and (311) planes of face-centered cubic crystalline of Pd, respectively (JCPDS standard 05-0681(Pd)). This indicated that the Pd particles in both Pd/C and the Pd/C–K_7 catalysts possess the face-centered cubic structure. The average sizes of the Pd nanoparticles in the Pd/C and Pd/C–K_7 catalysts are both 4.6 nm according to Scherrer equation [9,36].

Fig. 4 shows TEM images of the Pd/C and Pd/C–K_7 catalysts. As shown in Fig. 4A and B, Pd nanoparticles are well dispersed on the surface of carbon in both the Pd/C and Pd/C–K_7 catalysts. These results of the XRD and TEM images demonstrate that $K_7Co^{II}W_{11}O_{39}Sn^{IV}OH$ adsorbed on the Pd/C catalyst has no effect on the structure of the Pd/C catalyst.

3.2. Electrochemical performance analysis

A recent report indicates that Pd/C electrocatalysts easily lose a large amount of activity owing to the poisoning adsorption of CO_{ads} during formic acid electrooxidation [37,38]. Based on CO-stripping voltammogram studies (Fig. 5), it is found that the electrochemically surface area of the Pd/C and Pd/C–K_7 are 35.11 and 26.12 $m^2\ g^{-1}$. The oxidation peak potential of CO oxidation at the Pd/C–K_7 negatively shift ca. 25 mV compared to that at the Pd/C.

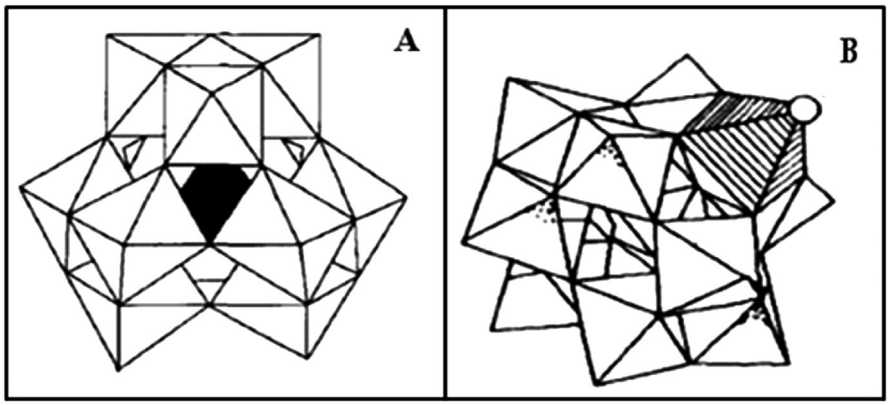

Fig. 2. Structure of (A) Keggin type and (B) Keggin type of Sn-substituted polyoxometalatate.

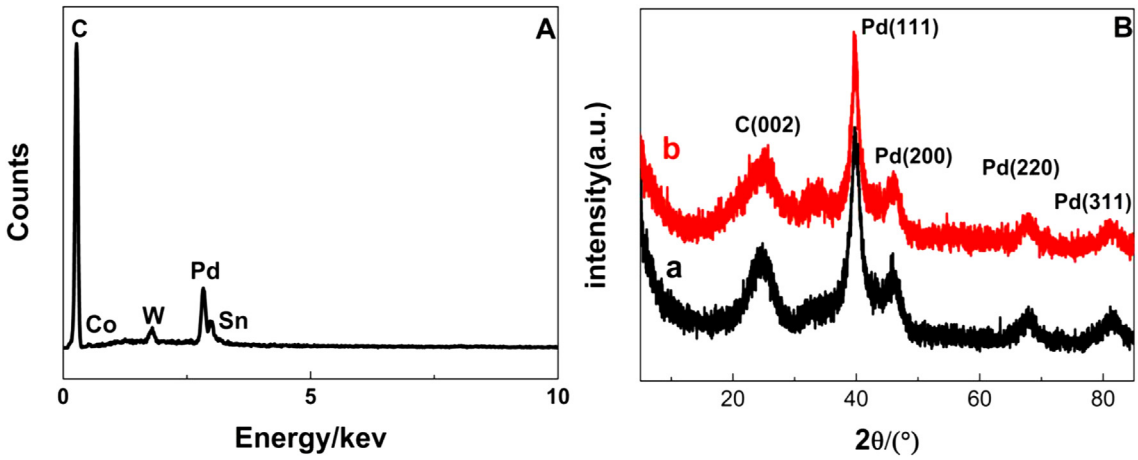

Fig. 3. (A) EDS spectrum of the Pd/C–K_7 catalyst; (B) XRD patterns of the (a) Pd/C and (b) Pd/C–K_7 catalysts.

The present CO-stripping tests indicate the dramatic diminution in the affinity of CO in Pd/C–K_7. According to previous reports, anions of polyoxometalate showed the ability to facilitate the electrooxidation of intermediate species such as CO_{ads} or the CO-like species during methanol electroxidation [12,34,39-41]. Therefore, the redox property of the $Co^{II}W_{11}O_{39}Sn^{IV}OH$ anion should have a positive effect on the removal of CO_{ads} oxidation for the Pd/C–K_7 catalyst. According to the triple-path mechanism of electrooxidation of formic acid (Scheme 1), the weak affinity of the Pd/C–K_7 catalyst for CO can facilitate the rate of the formic acid oxidation via the direct path, which also enhances the electrocatalytic stability of Pd/C–K_7 for formic acid electrooxidation.

Fig. 6A depicts the mass activities of the Pd/C and Pd/C–K_7 catalysts in the 0.5 M HCOOH and 0.5 M H_2SO_4 solution at the rate of 50 mV s^{-1}. The anodic peak current at the Pd/C–K_7 (363.2 A g_{Pd}^{-1}) is almost 1.9 times higher than that of Pd/C (189.0 A g_{Pd}^{-1}). Furthermore, the onset oxidation potential of formic acid oxidation on the Pd/C–K_7 shifts negatively ca. 34 mV compared to the Pd/C. In general, the mass activity can be taken as an index to assess the applicability of the catalyst for the formic acid oxidation [42,43]. Thus, the lower oxidation peak potential and higher oxidation peak current show that the Pd/C–K_7 catalyst has higher electrocatalytic performance than the Pd/C catalyst.

Fig. 6B displays the Tafel plots of log I vs. E for the formic acid oxidation at the Pd/C–K_7 catalyst and the Pd/C catalyst in electrochemical control region. In lower output current region, both curves keep consistent with Tafel linear relationship. Under the same output voltage, the Pd/C–K_7 catalyst shows a higher output current with respect to the Pd/C catalyst, namely, the slope of log I vs. E curve at the Pd/C–K_7 catalyst is smaller at the Pd/C catalyst. Moreover, the polarization over-potential at the Pd/C catalyst occurs at lower output current density. These results exhibit that the formic acid oxidation at the Pd/C–K_7 catalyst has a faster kinetic rate. The high protonic conductivity of the new polyoxometalate can facilitates the proton migration and promote electron transfer reactions during formic acid oxidation via the direct pathway.

It is well known that the specific activity of catalyst can effectively evaluate the actual value of the intrinsic activity. As observed in Fig. 6C, the peak current density (i.e., the specific activity) of the formic acid oxidation on the Pd/C–K_7 catalyst (13.9 A m^{-2}) is about 2.6 times higher than that on the Pd/C catalyst (5.3 A m^{-2}). Furthermore, the onset potential of formic acid oxidation on the Pd/C–K_7 catalyst shifts negatively ca. 34 mV compared to the Pd/C catalyst.

We further analyzed the turnover frequency (TOF) of the Pd/C–K_7 catalyst and the Pd/C catalyst for formic acid oxidation at 0.1 V according to Eq. (3) [44–46].

$$\mathrm{TOF} = i_k/neN_s \tag{3}$$

where i_k is the specific current density, n is the number of electrons transferred, e is elementary charge, and N_s is atomic surface density.

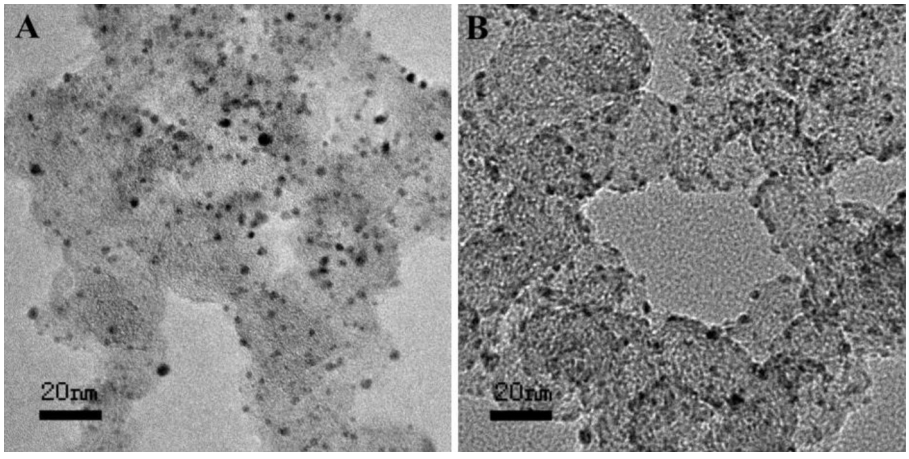

Fig. 4. TEM images of the (A) Pd/C and (B) Pd/C–K_7 catalysts.

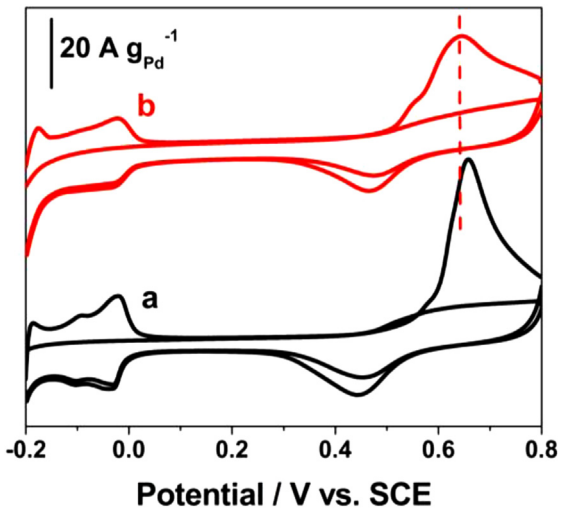

Fig. 5. Cyclic voltammograms of pre-adsorbed CO at (a) the Pd/C and (b) the Pd/C–K_7 catalyst in 0.5 M H_2SO_4 solution at the scan rate of 10 mV s^{-1}.

The TOF value gives the number of formic acid molecules formed per Pd surface site, assuming that all surface Pd atoms are active. The Pd/C–K_7 catalyst shows an enhancement in TOF than the Pd catalyst by a factor of 2.8 (2.5 atom^{-1} s^{-1} vs. 0.9 atom^{-1} s^{-1}) at 0.1 V potential. The improved activity of the Pd/C–K_7 catalyst for formic acid oxidation may be ascribed to the lower chemisorption of hydroxyl species, which offers more free active sites for formic acid oxidation.

To evaluate the electrocatalytic stabilities of catalysts, the chronoamperometry tests were conducted. Fig. 7A displays the chronoamperometric curves of 0.5 M HCOOH + 0.5 M H_2SO_4 solution at the Pd/C and Pd/C–K_7 catalyst electrodes at 0.10 V potential. It was observed that the current densities of formic acid oxidation at the Pd/C and Pd/C–K_7 catalysts electrodes are 30.18 and 63.96 A g^{-1} at 3000 s. They correspond to 9.15% and 17.18% current densities at 10 s at the Pd/C and Pd/C–K_7 catalyst electrodes, respectively. This fact indicates the durability of the Pd/C–K_7 catalyst is much better than that of the Pd/C catalyst.

Fig. 7B shows the current density versus cycle numbers curves for the cyclic voltammograms of 0.5 M HCOOH + 0.5 M H_2SO_4 solution at the Pd/C and Pd/C–K_7 catalyst electrodes. It was observed from Fig. 7B that although the current densities at the Pd/C and Pd/C–K_7 catalyst electrodes both decreased gradually with successive scans. After 500 CV cycles, the current density of the Pd/C–K_7 catalyst kept 43.6% of the initial value, two times higher than that in the Pd/C catalyst (22.1%). The above results are consistent with the results in Fig. 7A, demonstrating that the Pd/C–K_7 catalyst shows a greater stability for the electrochemical application than the Pd/C catalyst. The redox property of the $Co^{II}W_{11}O_{39}Sn^{IV}OH$ anion has a positive effect on the removal of CO_{ads} oxidation for the Pd/C–K_7 catalyst. The weak affinity of Pd/C–K_7 for CO facilitates the rate of the formic acid oxidation via the direct pathway, which also enhances the electrocatalytic stability of Pd/C–K_7 for formic acid electrooxidation.

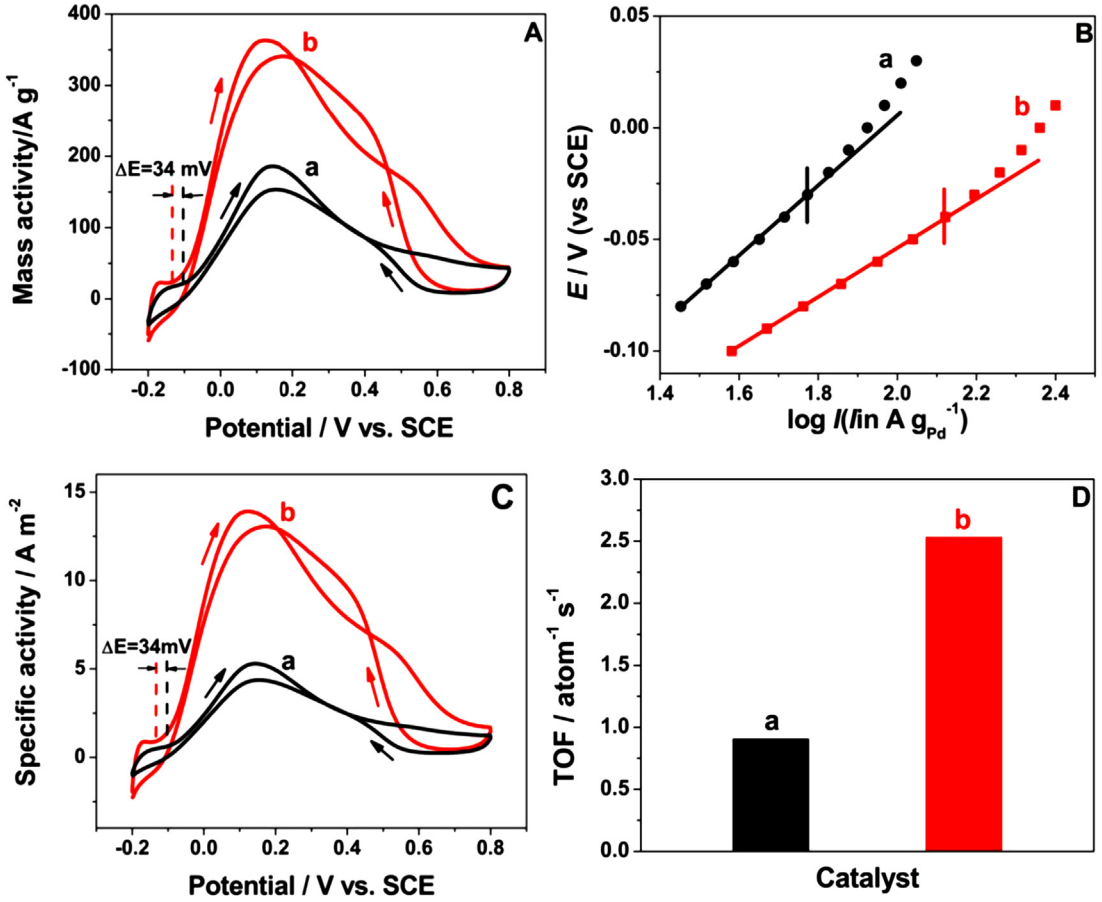

Fig. 6. (A) Mass activity of (a) the Pd/C and (b) the Pd/C–K_7 catalyst in 0.5 M HCOOH + 0.5 M H_2SO_4 solution at the scan rate of 50 mV s^{-1}; (B) Tafel plots of log *I* vs. *E* for the formic acid oxidation at (a) the Pd/C and (b) the Pd/C–K_7 catalyst in electrochemical control area; (C) specific activity of (a) the Pd/C and (b) the Pd/C–K_7 catalyst in 0.5 M HCOOH + 0.5 M H_2SO_4 solution at the scan rate of 50 mV s^{-1}; (D) the TOF of (a) the Pd/C and (b) the Pd/C–K_7 catalyst at 0.1 V.

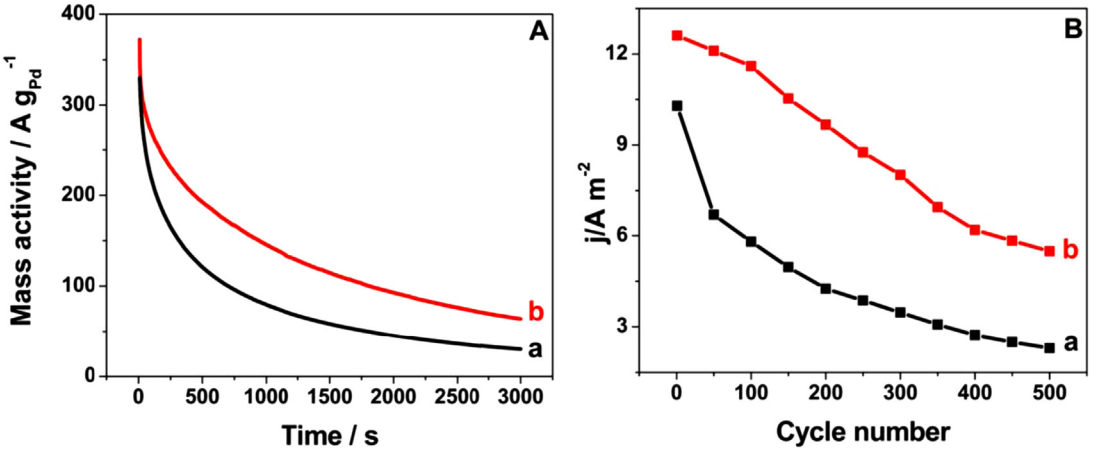

Fig. 7. (A) Chronoamperometry curves of (a) the Pd/C and (b) the Pd/C–K_7 catalyst in 0.5 M HCOOH + 0.5 M H_2SO_4 solution at 0.10 V; (B) the peak current density versus cycle numbers curves for the cyclic voltammograms of 0.5 M HCOOH + 0.5 M H_2SO_4 solution at the (a) Pd/C and (b) Pd/C–K_7 catalyst electrodes.

3.3. Decomposition of formic acid over two different catalysts

Fig. 8 displays the relationship curves between the time and the gas volume produced from the catalytic decomposition of formic acid over the Pd/C and Pd/C–K_7 catalysts in 0.5 M HCOOH + 0.5 M H_2SO_4 solution. The gas volume produced from the decomposition of formic acid over the Pd/C and Pd/C–K_7 catalysts in two hours are 31.5 and 5.8 mL, respectively. Previous research has shown that the main products of the decomposition of formic acid over the Pd catalyst are CO_2 and H_2. However, the products also contain a small amount of CO [47–49]. The catalytic decomposition of formic acid over the Pd catalyst wastes a lot of formic acid. Furthermore, CO from the decomposition of formic acid could poison the Pd catalyst to decrease the electrocatalytic performance of the Pd catalyst. The gas volume produced from the decomposition of formic acid over the Pd/C–K_7 catalyst is only 18.4% of that over the Pd/C catalyst, indicating that the Pd/C–K_7 catalyst can largely inhibit the decomposition of formic acid and then decrease the CO production. Therefore, the electrocatalytic stability of the Pd/C–K_7 catalyst for the oxidation of formic acid is much better than that of the Pd/C catalyst.

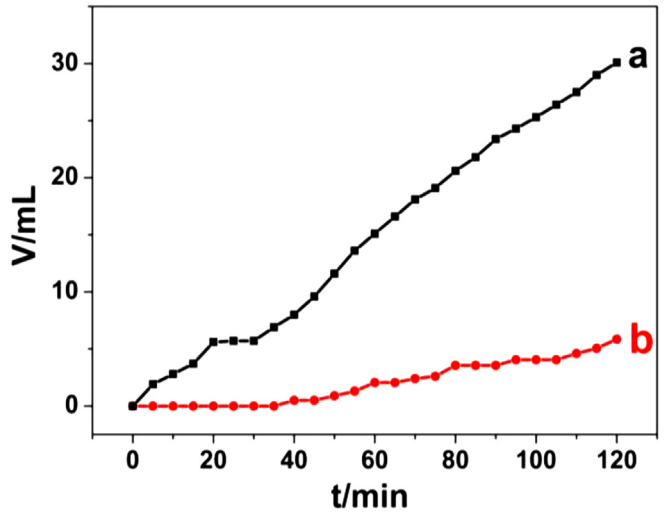

Fig. 8. The relationship curves between the time and the gas volume produced from the catalytic decomposition of formic acid over (a) the Pd/C and (b) the Pd/C–K_7 catalysts in 0.5 M HCOOH + 0.5 M H_2SO_4 solution.

4. Conclusions

In summary, the Pd/C–K_7 catalyst possesses the improved electrocatalytic activity and stability for formic acid oxidation. Due to the high protonic conductivity and redox property of $K_7Co^{II}W_{11}O_{39}Sn^{IV}OH$, the Pd/C–$K_7$ catalyst exhibits better electrochemical stability, superior CO tolerant ability and higher electrocatalytic activity over single-component Pd nanoparticles for formic acid oxidation. Based on the above results, the Pd/C–K_7 catalyst could solve the two major problems of DFAFC with the Pd/C catalyst: the decomposition of formic acid and the poor electrocatalytic stability. Thus, the Pd/C–K_7 catalyst has the good application respect in DFAFC.

Acknowledgments

The authors are grateful for the financial supports of National "973" program of China (2012CB215500), the National Natural Science Foundation of China (21073094, 21273116) and Natural Science Foundation of Colleges and Universities in Jiangsu Province (10KJB150007).

References

[1] C.H. Chen, W.J. Liou, H.M. Lin, S.H. Wu, A. Borodzinski, L. Stobinski, P. Kedzierzawski, Fuel Cells 10 (2010) 227–233.
[2] X. Yu, P.G. Pickup, J. Power Sources 182 (2008) 124–132.
[3] B. Fang, M. Kim, J.-S. Yu, Appl. Catal. B Environ. 84 (2008) 100–105.
[4] S. Murugesan, K. Myers, V. Subramanian, Appl. Catal. B Environ. 103 (2011) 266–274.
[5] J. Ge, W. Xing, X. Xue, C. Liu, T. Lu, J. Liao, J. Phys. Chem. C 111 (2007) 17305–17310.
[6] L. Zhang, L. Wan, Y. Ma, Y. Chen, Y. Zhou, Y. Tang, T. Lu, Appl. Catal. B Environ. 138–139 (2013) 229–235.
[7] Y.X. Chen, M. Heinen, Z. Jusys, R.J. Behm, Langmuir 22 (2006) 10399–10408.
[8] Y.X. Chen, M. Heinen, Z. Jusys, R.J. Behm, Angew. Chem. Int. Ed. 45 (2006) 981–985.
[9] Y. Chen, Y. Zhou, Y. Tang, T. Lu, J. Power Sources 195 (2010) 4129–4134.
[10] G. Zhang, Y. Wang, X. Wang, Y. Chen, Y. Zhou, Y. Tang, L. Lu, J. Bao, T. Lu, Appl. Catal. B Environ. 102 (2011) 614–619.
[11] J.L. Haan, K.M. Stafford, R.I. Masel, J. Phys. Chem. C 114 (2010) 11665–11672.
[12] X. Zhao, J. Zhu, L. Liang, C. Liu, J. Liao, W. Xing, J. Power Sources 210 (2012) 392–396.
[13] L. Lu, L. Shen, Y. Shi, T. Chen, G. Jiang, C. Ge, Y. Tang, Y. Chen, T. Lu, Electrochim. Acta 85 (2012) 187–194.
[14] Y. Tang, S. Cao, Y. Chen, T. Lu, Y. Zhou, L. Lu, J. Bao, Appl. Surf. Sci. 256 (2010) 4196–4200.
[15] M. Zhang, W. Zhang, T. Xiao, J.-F. Xiang, X. Hao, W.-H. Sun, J. Mol. Catal. A Chem. 320 (2010) 92–96.
[16] Sanjeev P. Maradur, G.S. Gokavi, Bull. Catal. Soc. India 6 (2007) 42–49.
[17] S.P. Maradur, S.B. Halligudi, G.S. Gokavi, Catal. Lett. 96 (2004) 3–4.

[18] M. Sadakane, E. Steckhan, Chem. Rev. 98 (1998) 219–238.
[19] Q. Wu, X. Sang, F. Shao, W. Pang, Mater. Chem. Phys. 92 (2005) 16–20.
[20] Q. Yang, H. Dai, J. Liu, Transit. Met. Chem. 23 (1997) 93–95.
[21] Y. Yang, J. He, X. Wang, B. Li, J. Liu, Transit. Met. Chem. 29 (2004) 96–99.
[22] L.A. Hongsen Wang, F.J. DiSalvo, Héctor D. Abruña, Phys. Chem. Chem. Phys. 10 (2008) 3739–3751.
[23] D.-H. Lim, D.-H. Choi, W.-D. Lee, H.-I. Lee, Appl. Catal. B Environ. 89 (2009) 484–493.
[24] X.H. Xia, Electrochim. Acta 45 (1999) 1057–1066.
[25] I. Bakos, S. Szabó, Electrochim. Acta 46 (2001) 2507–2513.
[26] H. Sun, J. Xu, G. Fu, X. Mao, L. Zhang, Y. Chen, Y. Zhou, T. Lu, Y. Tang, Electrochim. Acta 59 (2012) 279–283.
[27] C. Hsu, C. Huang, Y. Hao, F. Liu, Electrochem. Commun. 23 (2012) 133–136.
[28] J. Song, Z. Luo, H. Zhu, Z. Huang, T. Lian, A.L. Kaledin, D.G. Musaev, S. Lense, K.I. Hardcastle, C.L. Hill, Inorg. Chim. Acta 363 (2010) 4381–4386.
[29] J.-Y. Niu, Z.-L. Wang, J.-P. Wang, Polyhedron 23 (2004) 773–777.
[30] Y. Wang, B. Zou, L.-N. Xiao, N. Jin, Y. Peng, F.-Q. Wu, H. Ding, T.-G. Wang, Z.-M. Gao, D.-F. Zheng, X.-B. Cui, J.-Q. Xu, J. Solid State Chem. 184 (2011) 557–562.
[31] K. Nomiya, H. Murasaki, M. Miwa, Polyhedron 5 (1986) 1031–1033.
[32] J.E. Molinari, L. Nakka, T. Kim, I.E. Wachs, ACS Catal. 1 (2011) 1536–1548.
[33] B.A.M. Clemente-León, C. Mingotaud, C.J. Gómez-García, E. Coronado, P. Delhaes, Langmuir 13 (1997) 2340–2347.
[34] Z.P. Guo, D.M. Han, D. Wexler, R. Zeng, H.K. Liu, Electrochim. Acta 53 (2008) 6410–6416.
[35] J.C. Dawei Pan, Wenyan Tao, Lihua Nie, Shouzhuo Yao, Langmuir 22 (2006) 5872–5876.
[36] M.V. Martínez-Huerta, J.L. Rodríguez, N. Tsiouvaras, M.A. Peña, J.L.G. Fierro, E. Pastor, Chem. Mater. 20 (2008) 4249–4259.
[37] T.O. Hiroto Miyake, Gabor Samjeské, Masatoshi Osawa, Phys. Chem. Chem. Phys. 10 (2008) 3662–3669.
[38] X. Yu, P.G. Pickup, Electrochem. Commun. 11 (2009) 2012–2014.
[39] M.H. Seo, S.M. Choi, H.J. Kim, J.H. Kim, B.K. Cho, W.B. Kim, J. Power Sources 179 (2008) 81–86.
[40] L. Feng, X. Zhao, J. Yang, W. Xing, C. Liu, Catal. Commun. 14 (2011) 10–14.
[41] W.B. Kim, T. Voitl, G.J. Rodriguez-Rivera, J.A. Dumesic, Science 305 (2004) 1280–1283.
[42] W.P. Zhou, A. Lewera, R. Larsen, R.I. Masel, P.S. Bagus, A. Wieckowski, J. Phys. Chem. B 110 (2006) 13393–13398.
[43] W. Zhou, J.Y. Lee, J. Phys. Chem. C 112 (2008) 3789–3793.
[44] M. Jin, H. Zhang, Z. Xie, Y. Xia, Angew. Chem. Int. Ed. 50 (2011) 7850–7854.
[45] B.S. Yeo, A.T. Bell, J. Phys. Chem. C 116 (2012) 8394–8400.
[46] Z. Peng, H. You, J. Wu, H. Yang, Nano Lett. 10 (2010) 1492–1496.
[47] L. Zhang, Y. Tang, J. Bao, T. Lu, C. Li, J. Power Sources 162 (2006) 177–179.
[48] G.-Q. Lu, A. Crown, A. Wieckowski, J. Phys. Chem. B 103 (1999) 9700–9711.
[49] H. Hosseini, M. Mahyari, A. Bagheri, A. Shaabani, J. Power Sources 247 (2014) 70–77.